A human-centric approach to assess daylight in buildings for non-visual health potential, visual interest and gaze behavior

Maria L Amundadottir[1], Siobhan Rockcastle[1], Mandana Sarey Khanie[1] and Marilyne Andersen[1]

[1]Interdisciplinary Laboratory of Performance-Integrated Design (LIPID), School of Architecture, Civil and Environmental Engineering (ENAC), École Polytechnique Fédérale de Lausanne (EPFL), Switzerland

Corresponding author: Marilyne Andersen, E-mail: marilyne.andersen@epfl.ch

Abstract

This paper introduces a novel approach for the assessment of daylight performance in buildings, venturing beyond existing methods that evaluate 2-dimensional illumination and comfort within a fixed field-of-view in order to predict human responses to light concerning non-visual health potential, visual interest, and gaze behavior in a visually immersive scene. Using a 3D rendered indoor environment to exemplify this coordinated approach, the authors assess an architectural space across a range of view directions to predict non-visual health potential, perceptual visual interest, and gaze behavior at the eye level of an occupant across an immersive field-of-view. This method allows the authors to explore and demonstrate the impact of space, time, and sky condition on three novel daylight performance models developed to predict the effects of ocular light exposure using a human-centric approach. Results for each model will be presented in parallel and then compared to discuss the need for a multi-criteria assessment of daylight-driven human responses in architecture. A parallel and comparative approach can allow the designer to adapt the architectural space based on the program use and occupants needs.

1. Introduction

In pre-industrial times, humans spent a substantial amount of time outdoors, exposed to daylight during productive hours, which were primarily agricultural, constructive, or craft based and limited by the rise and set of the sun. In the 19th and 20th centuries, an increase in urban densification due to industrialized labor markets and advances in electric lighting, construction techniques, and indoor climate control technologies led to increasingly longer durations of indoor occupation. As a result, it has been estimated that the average human living between 41-46 N latitude spends ~2 hours outdoors per day [1]–[3]. These durations of time spent outdoors were progressively reduced over the last 8 years by ca. 0.5 hour difference [4], subjecting the non-visual and visual systems of post-industrialized urban residents to substantially lower illumination levels during daytime hours with increased electric lighting during the night.

While electric lighting can provide useful illumination for productive, social, and recreational activities when daylight is not present, humans have diverse and sometimes conflicting physiological and psychological needs [5]. Humans associate their state of wakefulness and activity with lit hours, while their sleep and rest cycles are commonly tied to darkness. This predictable change in the light environment is one of the most significant factors, which resets the human circadian clock within the built environment. In addition to regulating the circadian clock, light induces a range of direct non-visual (non-image forming) physiological and behavioral responses in humans, including but not limited to hormone production, alertness, and cognitive performance [6], [7]. Although certain visual tasks can be performed under relatively low light levels (as compared to the available outdoor illumination), such levels do not necessarily ensure adequate light to synchronize circadian rhythms to the 24-hour day or promote other physiological and behavioral non-visual responses. Our lighting environment must also support adequate luminous contrast to differentiate objects, read spatial depth, and appreciation of the luminous diversity, yet we also experience discomfort with excessive contrast and brightness in the field-of-view [8].

Humans perceive space as a 3-dimensional (3D) luminous scene, yet many of the daylight analysis methods currently used in modern practice assess light across a two-dimensional surface

(illuminance-based). This is due, in large part, to the energy concerns of the late 20th century, which identified daylight as an efficient alternative to carbon and energy-intensive electric lighting sources. Those methods that do address the field-of-view, were developed to assess discomfort due to excessive luminous contrast ratios within a fixed view position, often related to task-area [9]. While 2D illuminance does not account for the spatial composition of daylight across an occupant's field-of-view nor the vertical illuminance captured at the eye, those methods that do are limited in their assumption of a fixed [9] or arbitrary adaptive range view direction [10] and do not account for gaze responses which depend on lighting quality [11] or spatial configuration, i.e. window placement [12], room layout, or task placement [13]. The photometric parameters in the field-of-view which are underlying our current understanding of visual comfort are highly dependent on gaze-shifts which happen both voluntarily and involuntarily [14]. These methods do not account for behavioral gaze responses and leave us with limited capabilities to assess daylight from a visually immersive occupant point-of-view. In addition to this limitation regarding 2D surface vs. fixed or adaptive field-of-view, existing methods have not explored the effects of daylight on health or visual interest, which is essential to a holistic evaluation of daylight for its effects on occupant well-being.

The method presented in this paper will exemplify a human-centric approach to daylight evaluation. This approach will be carried out using a range of view directions from a single view position to simulate light distribution across a 360° span, which corresponds to an immersive field-of-view. High Dynamic Range (HDR) renderings with a wide fisheye specification will be used as inputs for health-based, perceptual, and gaze-driven performance models. From this single view position selected for the analysis, the authors will vary the time of day and day of year to evaluate the selected architectural case study across a range of view direction inputs. This occupant-driven approach does not seek to replace existing methods for evaluating illumination, but rather propose a human-centric approach for analyzing those aspects of daylight which are dependent on light received at the eye level: non-visual health potential, visual interest, and gaze response. These models, developed independently from ongoing research by the authors [15]–[17], will be applied for the first time to illustrate the need for multi-criteria daylight analysis and shift our attention to more human-centric performance assessment methods. Through the use of a common workflow, the three models will be

used to predict human responses to daylight, which then will be compared in parallel. This 'parallel comparison' is an approach that we adopted in this paper to assess daylight performance using these three predictive models. This type of analysis will allow the designer to use the results in an adaptive manner towards the architectural program of the space. Other possible analyses and interpretation methods are discussed further in the outlook of the work.

To rebalance daylight performance evaluation and integrate occupant needs with general illumination requirements, the authors have identified two target audiences for this work. Architects and lighting designers often express the desire to evaluate perceptual effects of daylight whose dynamic effects are differentiated from static electric sources [18]–[21]. This group is also increasingly more interested in health-based benefits and behavioral responses to daylight, particularly as they relate to clients in healthcare, education, and workplace design. The second audience for this work is owner-occupied clients who have a vested interest in providing healthy and visually stimulating environments for their inhabitants, especially when the effect of daylight may have a positive impact on their health, mood, or productivity.

2. Human-centered approach

When we transit from a spatially dependent (i.e. illuminance measurements across a 2D surface) to an occupant centric approach, three main challenges emerge: 1) how can we can predict human responses to light, some of which are subjective and can vary greatly depending on individual differences, 2) how does light affect human physiology, behavior, and emotional well-being, and 3) how can these predictions help us create a holistic assessment of the indoor environment as it impacts intended functional use and design intent. This section introduces three novel models: non-visual direct response, modified special contrast, and gaze response. These models have been developed in parallel by the authors with the goal of assessing daylight to predict health potential, visual interest, and glare-free zones within an occupants' field-of-view. Through a novel workflow described in Section 3, these three models will ultimately be adopted to represent a 360° immersive evaluation of space.

2.1. Non-visual direct-response (nvR_D) model

The non-visual direct-response (nvR$_D$) model was developed to compare the relative effectiveness of different light exposure patterns to have potential health benefits for humans. The development of such a model brings together disparate experimental studies that have demonstrated the impact of different light properties on non-visual responses in humans. The nvR$_D$ model integrates findings from these studies to introduce a novel simulation-based approach to predict the non-visual effects of light in architecture. While the optimal daily exposure of light and dark needed for promoting physiological and behavioral non-visual responses is currently unknown, there is evidence that light can have beneficial or degrading effects depending on the intensity, wavelength, duration, history, and timing of light exposure [7]. Daytime light exposure can reduce sleepiness and improve performance [22]–[25] but light exposure at night can suppress melatonin production resulting in circadian disruption [26]. Blue-enriched polychromatic light has been shown to be more effective than light at longer wavelengths because it enhances alerting effects and cognitive function [27]–[30], while full-spectrum light (i.e. daylight) stimulates visual and non-visual responses simultaneously and is therefore a good choice for daytime activities.

The discovery of the intrinsically photosensitive retinal ganglion cells (ipRGCs) [31] has led to a new understanding of how light affects human physiology and health and introduces a new dimension for architectural lighting design and engineering in buildings. The non-visual system adapts its response to changes in light intensity and spectral composition over a longer time period than the visual system. Current responses depend on past exposure and can extend over several hours, or even days [32]–[35]. At the same time, it provides new challenges in lighting performance evaluation, because these novel photoreceptors are the primary mediators of non-visual physiological and neurobehavioral responses to light, but can also function independently of classical photoreceptors, rods and cones used for seeing. This means that the human eye plays a dual role in detecting light and existing methods must be revised for the assessment of our lighting environment to meet the requirements of the non-visual system.

The nvR$_D$ model proposed in this paper is based on data obtained from experimental studies in which nocturnal melatonin suppression responses are studied under different lighting conditions (i.e. by varying light intensity, wavelength, duration, and history) [26], [34], [36]–[38]. These studies inform how the non-visual system responds directly to light exposure. For the purpose of this paper, we assume that direct light-suppressing responses of melatonin behave similar to other direct non-visual responses such as alertness in the absence of melatonin secretion. In order to differentiate between positive and negative effects of light, for example between daytime and nighttime exposure, a square-wave function corresponding to the sleep-wake cycle can be applied to evaluate the output signal. The validation of the model remains, whereas limited amount of data exists on comparable protocols and light exposures.

The inputs to the nvR$_D$ model are discrete time samples of effective irradiance $I(t)$ weighted to the sensitivity of the ipRGCs with $\lambda_{\max}$= 490 nm [39]. An earlier version of the model presented here consisted of 3 components [40], but the current approach will implement a preliminary extension by adding a 4th component L$_H$ shown in Figure 1 [15]. The intensity-response function $N(u)$ (Equation (5) in Appendix 1.1) was adapted from Zeitzer et al. [26], which demonstrated that 6.5 hours of 100 lx was enough to produce 50% of the maximum response in subjects that were previously exposed to dim light (< 10 lx) for an extended period of time. To account for this adaptation to light history [34], an additional feedforward term L$_H$ was added to the model that allows the system to remain responsive at lower and higher light levels. In turn, the half-maximum value increases with adaptation to higher light intensities but decreases with adaptation to lower light intensities (see Equations (6-8) in Appendix 1.1).

The two components: L$_1$ and L$_2$; reflect the temporal processing between a light stimulus and an output response. The area of these components is equal to unity, which means that the filters neither amplify nor reduce the total response integral. The output of a filter depends on both current and past inputs, which results in a time delay equal to the filter's length. These types of 'causal' filters apply well to the non-visual system with its dependence on current and past inputs [32], [34], [35] and are also less sensitive to intermittent (high temporal contrast) light exposure [36], [41].

The model outputs are time-sampled relative non-visual responses that reflect the direct light drive on the non-visual system. Thus the nvR_D model predicts how the non-visual system integrates light information over time depending on the dynamic light input. Predicting adaptations to temporal variations in light exposure are crucial for understanding how we can design our lighting environments with regard to the non-visual effects of light, because light spectrum and intensity can vary frequently in natural lighting conditions.
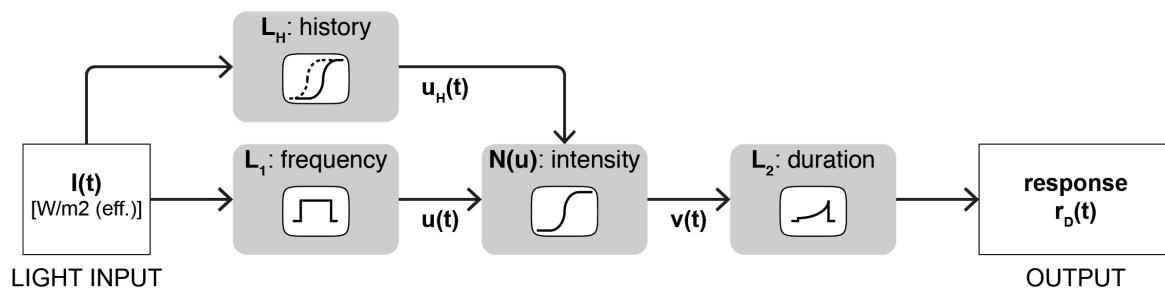
non-visual direct-response (nvR_D) model

Figure 1 – Diagram of the nvR_D model. The light input I(t) to the model is assumed to be ipRGC effective irradiance. The output response is the predicted direct non-visual response r_D(t). The four components of the model reflect the intensity-response curve (IRC) and the temporal processing between the light input and the output response.

2.2. Modified spatial contrast (mSC) as a predictor for visual interest

As mentioned towards the end of the previous section, natural lighting conditions can vary frequently based on temporal changes in the indoor environment. In spaces where daylight is a primary source of illumination, an occupant's visual perception of indoor space is largely influenced by the composition of light and shadow and the diverse temporal dynamics of this composition over time. While many architects and lighting researchers have identified the importance of these compositional impacts as qualitative design factors [18]–[20], there has been limited research into quantifying these contrast-driven effects into any kind of perceptual performance indictor [42]–[45]. Renderings are often used to assess the visual effects of daylight in architecture using qualitative intuition, but a single rendering (taken at one moment of time, under a single sky condition) cannot provide adequate information to evaluate the range of temporally induced effects that may occur over time. Even if we produce a time

series of renderings to adequately cover all daily and annual instances, we cannot compare the relative perceptual impacts of these effects between architectural spaces under a variety of sky conditions without some kind of objective measurement.

Simulation is a powerful tool for evaluating performance dynamics and a robust image-based measurement for predicting subjective impressions of daylight composition on emotional human-responses would help designers to understand where (within space) and when (over time) the effects of sunlight and shadow are likely to produce specific desired or undesired responses [46]. To predict occupant impressions of visual interest, the authors developed a quantitative model based on subjective ratings of visual interest in daylight renderings gathered through an online survey [16]. The survey used in this experiment asked participants to rank a selection of renderings: nine architectural spaces under three sunny sky conditions (modeled in Rhino, rendered using Radiance, and tone mapped using *pcond* to a standard Low Dynamic Range (LDR) computer display). Using seven-point semantic differential scales, subject ratings were then gathered for impressions of: low contrast – high contrast, uniform – non-uniform, unvaried – varied, diffuse – direct, simple – complex, calming – exciting, subdued – stimulating. Based on the authors' previous findings [46], it was suspected that some algorithms developed to measure compositional contrast, specifically those that measure local variations in brightness, could be used to predict subjective impressions. The ordinal responses collected from the semantic scales listed above were then compared to a range of existing and modified contrast algorithms to find which, if any, could be used to predict subject ratings.

Through an analysis of subject ratings it was found that rating pairs like 'calming – exciting' and 'subdued – stimulating' were highly correlated ($\rho = 0.98$) and could be collapsed into a single rating pair. Pearson correlation coefficients between subject ratings and contrast algorithms revealed that RAMMG, a local neighborhood contrast measure developed by Rizzi at al., had the strongest dependence to subject ratings of low contrast – high contrast. A modification of this algorithm, specifically the 5th pixel subsampling level (N=5) of input resolution 1488 x 1024 (hereafter called RAMM5), had the strongest dependence to subject ratings of diffuse – direct, simple – complex, calming – exciting, and subdued – stimulating. The authors selected calming – exciting ($\rho = 0.79$) because while this bi-polar semantic pair is not an exclusive representation of 'visual interest' the

authors determined that its correlation to ratings of stimulation and its strong dependence to the RAMM5 measurement made it possible to propose a predictive model. The authors found that for an image (of input resolution 1488 x 1024), RAMM5 could predict subjective impressions of calming – exciting using an ordered logit model [47]. This modified algorithm, referred to as modified Spatial Contrast mSC, is defined in Appendix 1.2. The cumulative predictive probabilities for each rating on the scale 1-7, from calming to exciting, best fit the equation

$$P(y \leq j) = \left(1 + e^{a_j - b \times mSC_5}\right)^{-1}, \qquad \forall j = 1, \dots, 6, \qquad (1)$$

where $b = 0.24$ is the corresponding effect parameter, $a = [-0.45;\ 0.84;\ 1.67;\ 2.82;\ 3.64;\ 4.81]$ the cutoff points. At level 3, the odds of achieving ratings 1-3 were significant at p<0.05. Rather than predicting the probability of a subject's response at each level, this paper will focus on a pair of thresholds for predicting impressions of 'calming' or 'exciting' derived from the ordered logit model and presented in Section 3.3.2.

Figure 2 shows the steps used to predict visual interest in the context of this paper, using the calming – exciting bi-polar scale. For each hemispherical fisheye rendering, the matrix of luminance values is first subsampled by halving the resolution in 5 subsequent steps. This reduced map of luminance values is then used to compute local variations $c_{i,j}$ in brightness between each pixel and it's eight neighbors, using a weight α applied to each neighbor, element wise. The average $c_{i,j}$ taken across all resulting values of the matrix is then calculated to produce the resulting mSC$_5$.

The full results of the online experiment and the analysis used to generate the predictive model presented here have been published in more depth by the authors in [16], [46], but the integration of these thresholds into an immersive analysis allows us to see, for the first time ever, the effect of view direction on predictions of visual interest in an architectural space. Whereas the authors previous work focused on predicting impressions using a 2D rectangular rendering with a fixed view direction, this paper allows for the immersive assessment across an entire 360° view range, revealing the effects of orientation and architectural composition on impressions of excitement and calm.

visual interest

for each HDR rendering

image is subsampled down in resolution

W

$\frac{W}{2^5}$

H

$\frac{H}{2^5}$

level 1

level 5

$c_{i,j}$ is computed as difference between $p_{i,j}$ and neighboring pixels with weight α applied to difference between pixels, element wise

$$\alpha = \frac{1}{(4+2\sqrt{2})^x}$$

$\frac{\sqrt{2}}{2}$	1	$\frac{\sqrt{2}}{2}$
1		1
$\frac{\sqrt{2}}{2}$	1	$\frac{\sqrt{2}}{2}$

$p_{i-1,j+1}$	$p_{i,j+1}$	$p_{i,j-1}$
$p_{i-1,j}$	$p_{i,j}$	$p_{i+1,j}$
$p_{i-1,j-1}$	$p_{i,j-1}$	$p_{i,j-1}$

$= \boxed{c_{i,j}}$

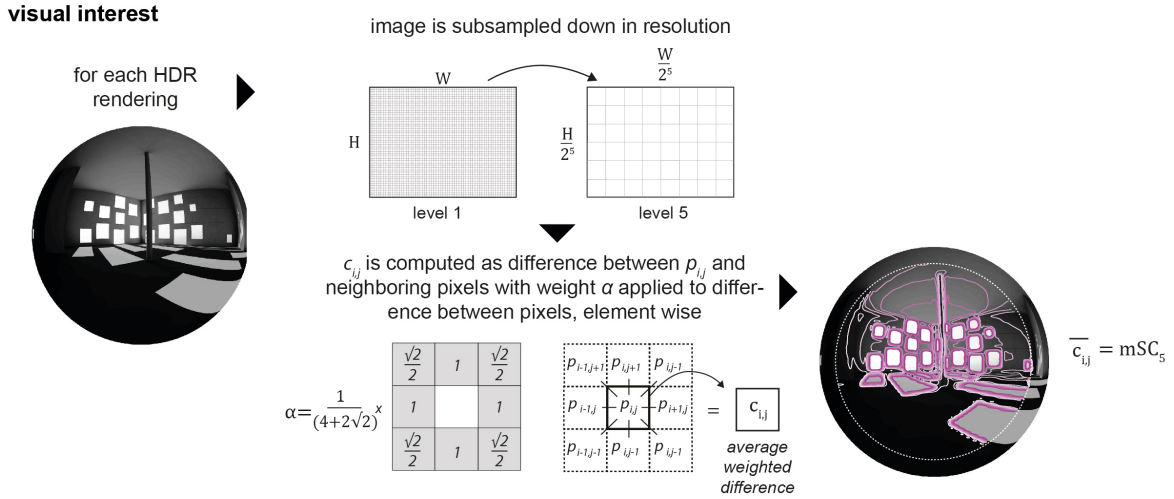*average weighted difference*

$\overline{c_{i,j}} = mSC_5$

Figure 2 – For each HDR rendering, the image is subsampled down. Local luminance variations are then computed for each pixel and its eight surrounding neighbors to create a matrix of local variations in compositional brightness. From this new matrix, the average mSC_5 is then computed.

2.3. A preliminary gaze responsive light-driven (GR$_L$) model

The two sections above highlight the importance of daylight for health and visual perception where high levels of direct access can be used as an aid to improve alertness, performance, sleep, and mood; and for spatial appreciation in terms of visual interest. Nevertheless, introducing high levels of daylight penetration in buildings can create limitations for our visual comfort and performance. Existing methods for visual comfort analysis driven by daylight evaluation that are based on perceived light at the eye, link quantifiable photometric measurements in the field-of-view, visibility and subjective preferences [48]. This information is used to predict and eliminate visual discomfort in space to ensure visual comfort and hence, higher visual performance.

The limitation of these methods is encountered with each gaze shift of the eye, where luminance distributions and consequent photometric measurements within the field-of-view at the eye level change, requiring the visual system to re-adapt to the new situation depending on the type of gaze movement [49]. Knowing that the luminance distribution across different regions of the field-of-view [50], [51] and the relationship between these regions can contribute to subjective visual comfort perception [52] and behavioral objective responses [53], [54], [55], the changes in this relations caused by gaze shifts should be observed. Nevertheless, the assumption behind existing prediction metrics is

that gaze direction is fixed and directed towards a task area. A few studies have investigated the relationship between gaze shifts and building-induced visual context such as windows [56] or compositional effects of light [49], [53], [57]. These studies deny the fixed assumption of gaze direction, suggesting that gaze rests on vertical and horizontal planes and is not fixed exclusively on the task area [58]. While certain luminance ratios in the field-of-view have been recommended to avoid constant visual re-adaptation for better visual performance [49], extending gaze direction to an angular adaptive zone is also suggested [10]. However, the natural gaze behavior in relation to light and visual discomfort is still largely unknown.

In order to overcome the fixed-gaze assumption, gaze behavior was studied in a series of experiments (implicitly constrained by real world luminous conditions) in a controlled simulated side-lit office space [17]. In these experiments, the gaze behavior for each participant was recorded using eye-tracking techniques and daylight dynamics were measured using HDR imaging techniques. A gaze photometry measurement method was developed by integrating recorded light variations from the luminance images coupled with mobile eye-tracking methods for recording gaze responses [59]. The findings of this study showed significant statistical relations between luminance variations and the recorded shift of gaze direction with a clear attraction and avoidance in behavior resulting from light and view outside the window [11]. It was found that while a subject's gaze would avoid extreme luminance levels, it could tolerate higher luminance levels when attracted to the outside view when the participants were not engaged in a visually demanding task. On the other hand, when performing a visual task gaze was attracted to the devices that support working tasks independent from the lighting configuration [13]. The later case implies that task regions override other affective parameters on gaze behavior. Knowing the importance of the task area, identifying regions that are more gaze responsive as a result of the light variations in the field-of-view (avoiding or attracting regions) can thus give us a better understanding on where to locate a demanding visual task within the room. Both findings reveal the importance of lighting compositions in the field-of-view and its impact on gaze behavior for enhancing the visual quality of the interior space. Based on the collected data and with focus only on the avoidance behavior, a preliminary gaze model was developed and will be applied in this paper for

the very first time to predict angular shifts in relation to a definition of luminance contrast in the field-of-view.

The preliminary model predicts 'gaze responsive zones' based on an initial gaze point vp and direction $\vec{v_F}$ (Figure 3). The gaze responsive zones are areas in space where gaze has shifted as a result of luminance contrast in the field-of-view. As opposed to the algorithms used to predict localized contrast values in Section 2.2, the luminance contrast described here is defined as an inverse relation between the brightest regions in the field of view (defined as glare impact (GI)) and adaptation levels at the eye (introduced by average luminance of the pixels (L_m)) and angular distance to glare from a initially given "fixed" view ($\Delta\theta_{FG}$)). Based on this model, the angular gaze shift $\Delta\theta_{RG}$, which is defined as the distance between a responsive gaze vector and the brightest region of the field-of-view, can be predicted. The equations for the GR_L model, GI, and L_m are listed in Appendix 1.3.

The predicted angular gaze shift $\Delta\theta_{RG}$ is then used to generate the rotation matrix (Equations (17 – 19) in Appendix 1.3) for obtaining the responsive gaze vector $\vec{v_R}$. The direction of the angular gaze shift is defined in the opposite direction to the brightest glare source vector $\vec{g}_m$ in relation to the initial fixed view $\vec{v_F}$.

The ultimate goal for the application of this model would be to identify a range of view directions within an architectural space where occupants can experience glare-free daylighting. This model, while preliminary, has been adopted in this paper to show the possibilities for application, while further validations are required in order to verify its robustness.
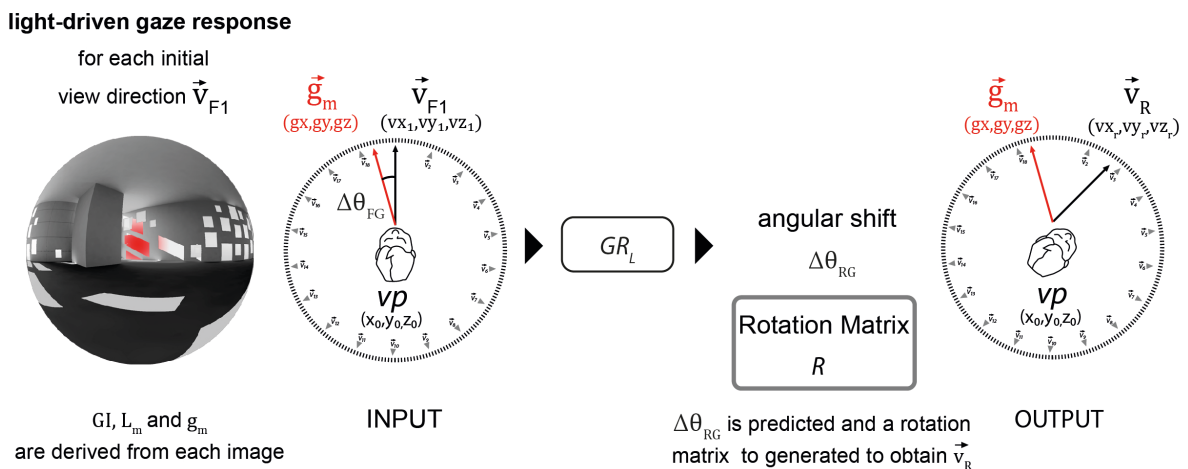

light-driven gaze response

for each initial view direction $\vec{V}_{F1}$

GI, L_m and g_m are derived from each image

INPUT

GR_L

angular shift $\Delta\theta_{RG}$

Rotation Matrix R

$\Delta\theta_{RG}$ is predicted and a rotation matrix to generated to obtain $\vec{v}_R$

OUTPUT

Figure 3 – Diagram showing the first representation of the GR_L model. This model, which is derived from an experimental study with combined eye-tracking and HDR imaging techniques, predicts the angular shifts based on luminance contrast in the field-of-view.

3. Simulation workflow and setup

Section 3.1 will describe the integration of these three models into a novel human-centric approach to lighting simulation, through which we can begin to move beyond conventional spatial methods and address human responses to daylight in architecture. The case study selected to demonstrate this approach will be introduced in Section 3.2 together with the simulation parameters select for analysis. In Section 3.3, threshold values chosen for the different performance indicators based on the models introduced in the previous section will be identified, with assumptions to the maximum and minimum acceptable values further explained.

3.1. Simulation workflow

To assess the human-centric impacts of daylight from an occupant view(eye) position, the following workflow has been established. Within a given 3D digital model, a view point is selected to represent an occupant's position in space. From this view position, a series of spherical renderings are generated for each time and date selected for analysis. These spherical renderings are simulated in Radiance from an initial view point: one tonemapped set (using *pcond*) to assess visual interest and one untonemapped set used to derive the necessary photometric parameters (using *evalglare*) for predicting health potential and gaze responses. The tonemapped and untonemapped spherical renderings are then "unrolled" using the *pinterp* function in Radiance using the same view point and 18 initial view direction coordinates resulting in 18 hemispherical fisheye HDR images. This workflow shown in Figure 4, enables the rapid production of hemispherical fisheye images for any number of view directions from a single view point in space. This is made possible because the full 360° view range is rendered in the spherical image and allows for a multi-directional evaluation of the selected space from the given view point. The hemispherical fisheye images are then used as input to

the three predictive models (nvR$_D$, mSC, and GR$_L$ models) introduced in Sections 2.1 – 2.3 using the threshold values described in Sections 3.3.1 – 3.3.3 to evaluate daylight impact.
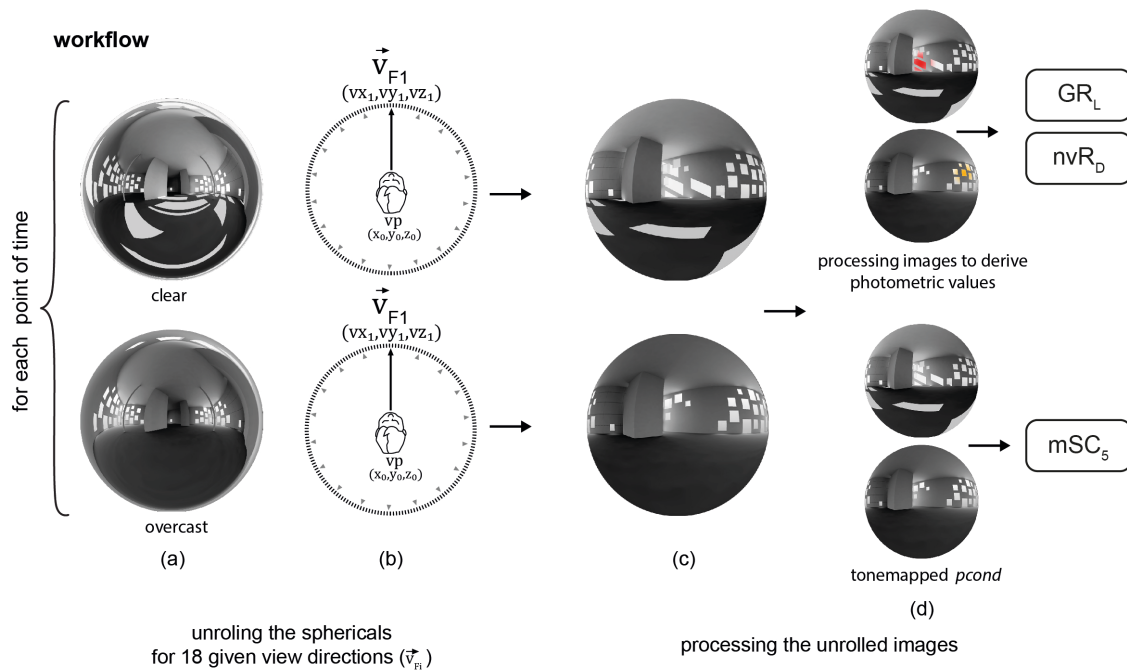

Figure 4 – A schematic of the proposed workflow. (a) Spherical renderings from a given view point in space vp (x,y,z). Tonemapped and untonemapped spherical renderings are generated for a desired time, date, and sky type. (b) 18 view directions with an interval of 20° are considered as initial view directions. The unrolling of each spherical image results in 18 hemispherical HDR images. (c) Two examples of unrolled HDR hemispherical fisheye images. (d) The untonemapped (on top) and tonemapped (on bottom) HDR images are processed to derive the relevant photometric quantities for inputs to nvR$_D$ and GR$_L$ models and mSC models.

3.2. Simulation setup and case study building

SANAA's Zollverein School of Management in Essen, Germany (latitude: 51.5°N, longitude: 7°E) shown in Figure 5(a) was selected as the case study for this paper due in part to its unique distribution of windows in each of the four cardinal directions. This 35-meter cube was completed in 2006 and contains of a series of vertically stacked single, double, and triple height educational spaces. The case study was selected as a representative example of contemporary architecture, where daylight and an understanding of its dynamics have played an important role in its design. Using an architectural case study where daylight considerations were central to the architect's design intent allows us to discuss

the role of architecture on human responses to this light stimulus within the interior. The façade is composed of asymmetrically distributed square windows, which filter sunlight and provide framed views of the surrounding landscape. The authors have selected a centrally positioned view point in a triple-height mixed-use space (first floor level), with eye-level at 1.67 meters from the floor. Eighteen default view directions have been used to generate hemispherical renderings in 20° even radial increments in order to cover the entire visual field (Figure 5(b)).

Using 6 daily moments, starting at 8h and running in 2-hour increments until 18h, we have chosen to assess the typical work-study period for an academic building of this type. These 6 daily moments are repeated across 4 semi-annual days, representative of a symmetrical half year (Figure 5(c)). For each point in time, a spherical rendering is generated under CIE clear and CIE overcast sky models using the rendering parameters and material definitions in Tables 1 and 2, respectively. In these simulations no shading system were considered.

The scene is rendered in neutral gray scale colors, to ensure that the spectral power distribution of the assumed daylight source (CIE standard indoor illuminant ID65 [60]) does not change due to color in the materials before it reaches the eye. This is done to overcome the limitations of existing daylight models that cannot accurately predict the spectral distribution received at the eye and are limited to photometric quantities. Acquiring this information is necessary in order to make accurate predictions of non-visual responses, as the spectral sensitivity of the non-visual system is more sensitive to blue light in comparison to the visual system.

Table 1 – Non-default rendering parameters used as an input to *rcontrib* in Radiance

dt	dj	ds	ab	aa	ar	ad	as	lr	lw	pj	ps	pt
0.05	0	0.15	3	0.1	512	4096	2048	8	5e-3	2	0.05	0

Table 2 – A list of Radiance materials used in this simulations study.

Materials	Description
GenericInteriorWall_50	Diffuse reflectance of 50%
GenericCeiling_70	Diffuse reflectance of 70%
GenericFloor_20	Diffuse reflectance of 20%
Glazing_DoublePane_Clear_80	Clear glazing with visual transmittance of 80%; visual transmissivity of 87%; SHGC = 0.72 ; U-Value = 2.71 W/m^{2}K

simulation setup
Zollverein by SANAA

(a) 3D model

(b) view position (*vp*)
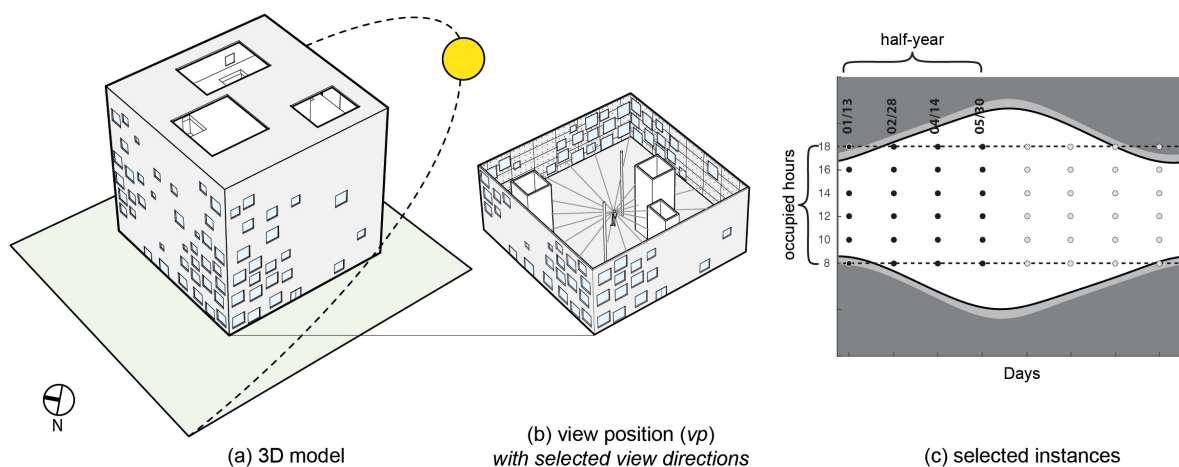*with selected view directions*

(c) selected instances

Figure 5 – The simulation setup. (a) 3D model of the case study building: SANAA's Zollverein School of Management in Essen, Germany. (b) The view position is located in the center of the space with eighteen view directions evenly distributed radially at 20° increments to cover the entire visual scene. (c) An overview of simulated time and dates selected based on occupied hours and to represent daylight hours over the year.

3.3. Analysis workflow and performance indicators

Predefined thresholds explained below were applied to the hemispherical fisheye renderings generated under both clear and overcast sky conditions to compare non-visual health potential and subjective predictions of visual interest across a range of view directions (for each of the 20° radial increments selected for this study). The responsive gaze model introduced in Section 2.3 is used to predict dominant view direction(s) or gaze responsive zones in relation to unwanted contrasts in the field-of-view.

3.3.1. Non-visual health potential

The nvR_D model introduced in Section 2.1 is sensitive to changes in light intensity, wavelength, and temporal characteristics of the input light signal. Offering an improvement over simple threshold values [60], this model also introduces a new challenge in that it is not a point in time evaluation

16

where the response depends on the history of past inputs. The nvR_D model outputs a smoothed delayed version of the input light signal, which in this paper is derived from the vertical illuminance at eye level. The spectral distribution of the daylight simulated in the scene is assumed to not vary with time or sky conditions, therefore the inputs to the model can be corrected to represent to the sensitivity of the ipRGCs [60]. Vertical illuminances are calculated from the HDR images for each hemispherical HDR image and then converted into ipRGC effective irradiance. This is achieved by assuming spectral power distribution of CIE standard indoor illuminant ID65.

The non-visual cumulative response R_D was computed for different light intensities and durations of continuous light exposure to illustrate the non-linear relation between irradiance and exposure duration. The obtained results of the cumulative response R_D outputs are shown in Figure 6(a) for illuminant CIE ID65 using contour lines to represent the change in response from 0 to 9. For lower light intensities, the rate of accumulation with increased duration is slower, compared to higher intensities where the response has saturated. This table of results is only valid for comparing continuous light exposure of fixed intensity and duration, where intermittent patterns must be simulated for every case.

As a proof-of-concept for this paper, a threshold was estimated based on a study by Phipps-Nelson et al. [22] to evaluate the potential health benefits of the simulated light exposure. It was shown that daytime polychromatic light exposure of 1000 lx (equivalent to 824 lx of CIE ID65 and equal to 2.7 W/m^2 effective) for the duration of 5 hours reduced the impact of sleep loss on sleepiness levels and performance, as compared to dim light. The threshold was obtained by simulating this 'reference' profile which gave the cumulative response $R_D = 4.2$ as illustrated in Figure 6(a). This threshold was established as a reasonable criterion for a university building because the experiment was conducted on young healthy adults that had undergone 2 nights of sleep restriction. Figure 6(b) shows a graphical representation of how spatial performance can be visualized by view direction using a radial plot. The cumulative response value is plotted for every view direction (and sky condition), where the orange fill represents the target performance. Depending on the goal of an analysis for a given set of design intentions, indicators of non-visual health potential may differ, i.e. what is healthy may change between scenarios or occupants' profile (age, chronotype, etc.).

In this paper, only occupied hours are taken into consideration and thus daylight hours before or after the defined period are not analyzed. When evaluating light in hours close to wake time and sleep onset, one must take into account circadian phase-shifting but as the building is occupied during daytime hours it is not possible to make predictions on circadian health (as it requires a full 24-hour light profile). It is assumed that the occupant enters the building at 8h and leaves at 18h. In order to track the non-visual light consumed over time, the response is integrated for comparing the potential benefits of different light exposures on health, but first, the data points at 2h intervals are interpolated linearly at 0.1 h step size to provide the necessary inputs to the nvR_D model. At every 2h increment the cumulative response is reported and evaluated against a predefined threshold ($R_D = 4.2$).
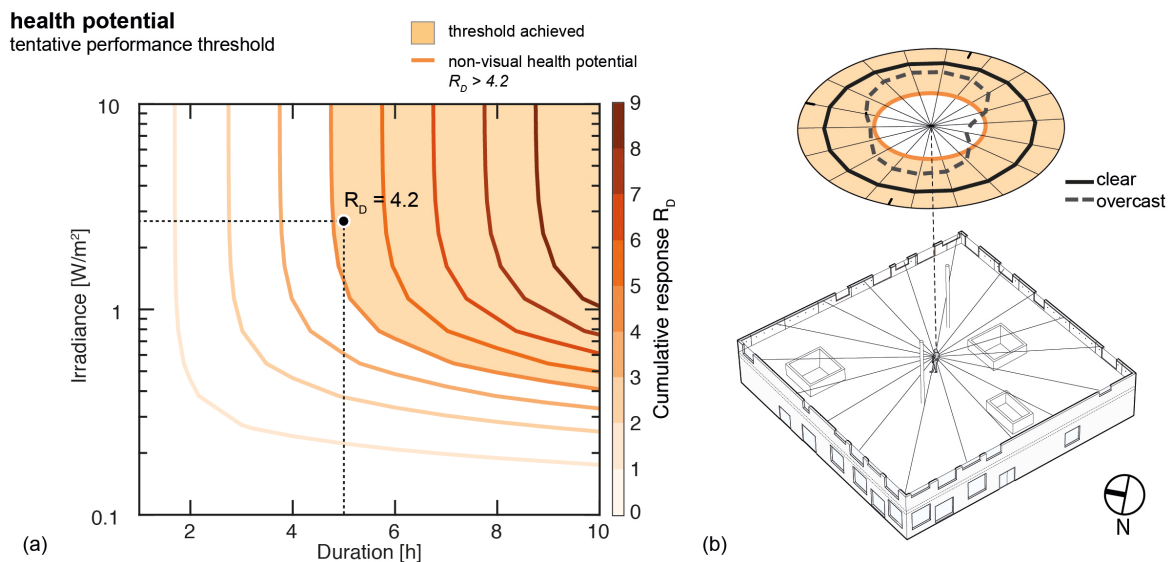

Figure 6 – (a) The cumulative response R_D as a function of irradiance and light exposure duration. The simulated reference profile resulted in $R_D = 4.2$, which was selected as the threshold for identifying the potential of light to induce health benefits within the selected space. (b) A visual representation of the daylight performance within a space. The performance target RD > 4.2 is represented with an orange fill and the predicted performance for each desired view direction is plotted as a line using a radial plot.

3.3.2. Visual interest

As described in Section 3.1.2, the mSC model presented in this paper was derived from an experiment, which compared subjective ratings of 2D tone-mapped renderings to a range of contrast algorithms [16] and found that one modified algorithm could be used to predict ratings of calming - exciting.

From the distribution of ratings across the renderings in this experiment, the authors used an ordered logit model to predict the probability of subject responses at each level, from 1–7. From this analysis, it was found that cumulative responses were significant at level 3, i.e. the odds of achieving a rating of 1-3 were significant at $p<0.05$. For the purpose of this paper and from the finding of this analysis, we decided to group levels into either calming, neutral, or exciting. Using this model, the authors have identified two thresholds for predicting occupant impressions of calming (j=3) and exciting (j=4). In the range 0-20 mSC_5, we obtain these thresholds by solving for mSC_5 in Equation (1) and by setting the predictive probability to 50%, which gives us

$$mSC_5 = (\ln 1 - a_j)/b, \qquad\qquad (2)$$

where N=5 stands for level 5. As seen in Figure 7(a), the obtained threshold values are 6.96 (j=3) and 11.75 (j=4) respectively for calming and exciting. mSC values between 6.96 and 11.75 are therefore established as neutral as there was no clear distribution on either side of the rating scale. Once computed for each view direction, results for clear and overcast skies can be overlaid using an angular plot to visualize results between sky conditions and across the occupant's view range (Figure 7(b)). Although these thresholds were derived from subjective data on 2D images with a horizontal and vertical view range of 80 x 60 degrees (respectively), the mSC for each image is computed as an average of local values taken across the composition. As such, the same thresholds for average mSC can be applied to images with a different set of view parameters, such as the 180° fisheye selected for this paper because the average and not the sum of values is used to determine subject responses. Future work in the development of this model will look at subject predictions gathered from across a 3D image to further refine the prediction model and its relationship to immersive viewing environments.
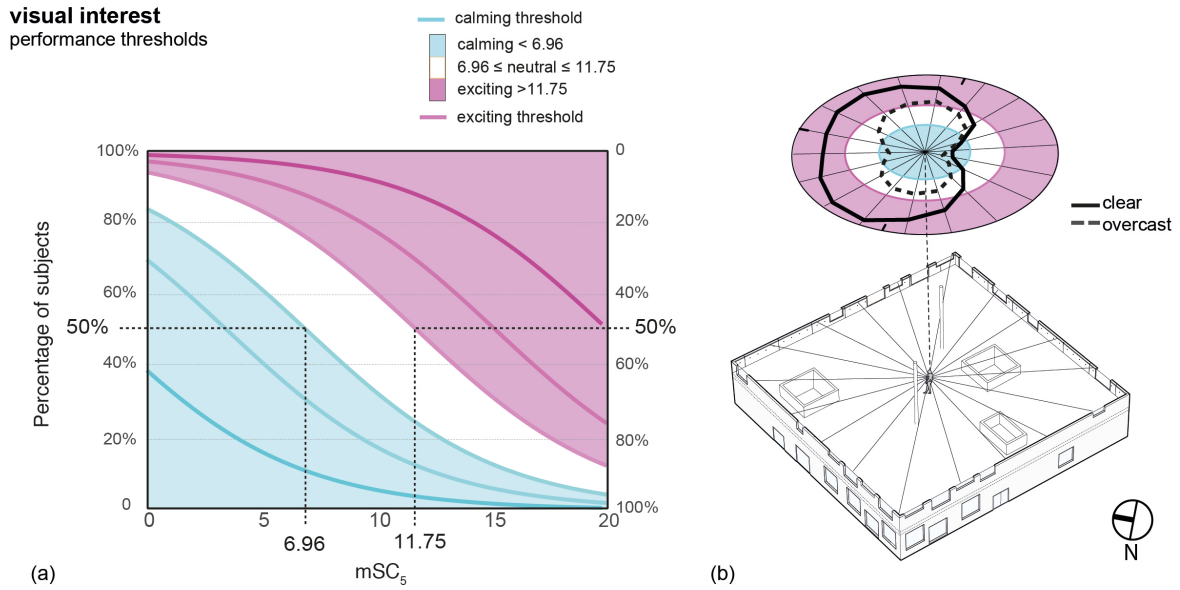
Figure 7 – Calming and exciting responses are determined using the thresholds at (a) 6.96 (j=3) and 11.75 (j=4), where 50% or more of the population is predicted to rate that rendering on one side of the scale. A point-in-time overlay of results for clear and overcast skies is shown in (b) to visualize the impacts of the case study and view directions on predicted responses.

3.3.3. Gaze frequency distribution

The GR_L model predicts the angular shift avoidance from high intensity glare sources weighted by their size with reverse relation to the glare source angular distance from a given view direction $\overrightarrow{v_F}$, and the eyes adaptation levels at the same given original view position vp of that view direction. Here, each rendered fisheye image generated at 18 initial view directions from one view point in space was processed using a Radiance-based tool *evalglare* [61]. Using this tool, the average luminance L_m of each processed image was derived as well as glare source intensity L_s, glare vector $\overrightarrow{g_m}$ coordinates, and glare source size ω_s. The glare sources detection parameters [62] were set to default values of 0.2 for search radius and average luminance of the image as the reference threshold. The glare impact GI and angular distance $\Delta\theta_{FG}$ between initial line of view direction and the center of the maximum glare source patch in the field of view was calculated as inputs to the GR_L model. GR_L Model predicts the angular shift from the maximum glare source in the field of view. The avoidance from the glare source vector is implemented through an algorithm that checks the position of the glare source direction in

20

relation to the view direction. In a subsequent step a sign function is considered when using the predicted angular shift to rotate the view direction coordinates. For each initial view direction $\overrightarrow{v_F}$, a rotation matrix was generated and employed to obtain the predicted shifted response gaze vector $\overrightarrow{v_R}$.

The responsive gaze directions are represented on an angle histogram showing the distribution of values grouped according to their new 'angular shift' avoidance at each time of day (Figure 8). The histogram demonstrates the frequency of gaze distributions over space for a fixed bin size of 6 (Figure 8(a)). The bin size of six is chosen here for the data sample of 18 in order to give a minimum frequency of 3 in each bin in case of even distribution. The highest frequency of gaze directions in the 360° range indicates the dominant 'gaze responsive zone' (Figure 8(b)). The spatial and temporal effect of the chosen architecture on the gaze distributions could be observed quantifying the variance between the resulting frequencies (Figure 8(c)). The effect of these two parameters where then analyzed using a 2-way analysis of variance (ANOVA).
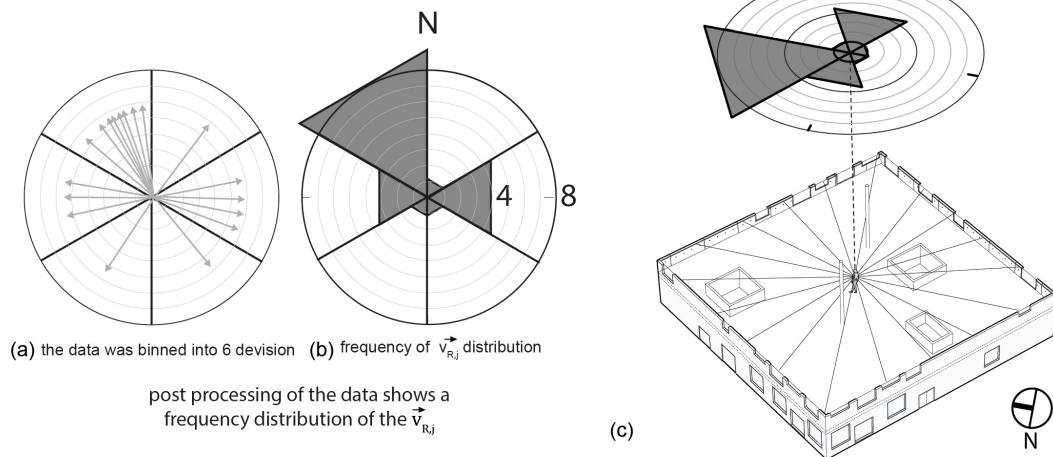

Figure 8 – The schematic illustrates the process that leads to obtaining dominant gaze responsive zones. Depending on the contrast variations in field of view (18 fisheye images for each view direction), the model predicts shift of the respective view direction if any: (a) The distribution of predicted view directions are generated over the space for each hour during the occupancy hours, (b) the shifted view directions are then binned over 6 zones of space and the frequency of their distribution is calculated to show the gaze responsive zones.

4. Results

In this chapter we will demonstrate the application of the three human responsive prediction models for daylight assessment using the proposed case study introduced in Section 3.2. The results for non-visual health potential, visual interest, and gaze response are presented using angular plots to enable the comparison of the 'full immersive view'. These results are analyzed for each daylight indicator and then compared and discussed in relation to each other.

4.1. Non-visual health potential

The radial plots in Figure 9, with days of the year represented row-wise and time of day column-wise, show the cumulative non-visual response over time during occupied hours for the two sky conditions: clear and overcast. At every 2h time step the cumulative response is reported assuming that the light exposure starts at 8h to illustrate the total light dose accumulated over the day. It is important to note that the results show the cumulative response starting from 8h. If a person would enter the building at 12h, for example, the results will be different due to their previous exposure in other light environments. The non-visual health potential is reached if the cumulative responses passes the threshold of $R_D > 4.2$, marked with a yellow fill. After 6h of continuous light exposure, the threshold is achieved for April 14 and May 30 under both clear and overcast sky conditions. The effect of view direction (i.e. space) is more apparent for overcast sky, as the clear sky conditions result in an even outcome in all view directions, because the light intensity exceeds saturating intensity-response values (> 2.7 effective W/m^2, which equals c.a. 1000 lx). For shorter and darker days, the accumulation is slower than for longer and brighter days. The rate of the cumulative response is slower for February 28 compared to April 14 and May 30, as seen in Figure 9 by comparing the distance between lines. After 14h, the threshold is exceeded for most cases except for January 13. The last two hours of January 13 and February 29 do not contribute much to the overall daily response, because winter days are shorter.

Evaluating a time series of light exposures at fixed sensor point location and gaze may be considered as overly simplistic as humans change location in space and alter their view direction as time passes. On the other hand, it is challenging to predict movements of occupants and their interaction with the built environment. As the aim of this paper is to evaluate the lighting distribution

22

across an exemplary field-of-view, the sensor point location was fixed. In order to evaluate the

occupant experience within space, different sensor points can be sampled over space and time to

represent occupant behavior. As the non-visual system integrates light information over time,

assumptions regarding the occupant and its behavior will have a large impact on the simulated results.
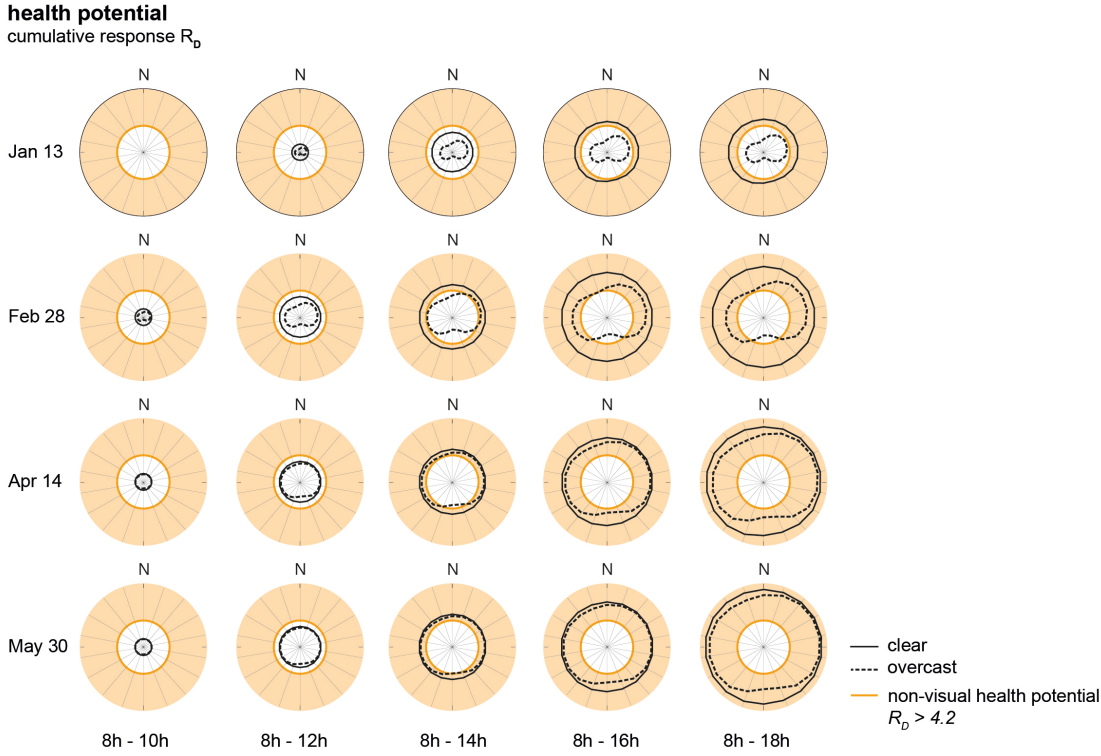
health potential
cumulative response R_D

Figure 9 – Radial plots showing the results for non-visual health potential. The cumulative response

R_D is shown at 2h increments of time. At time 14h, i.e. after 6 hours of continuous light exposure, the

threshold of $R_D > 4.2$ is achieved in most cases.

4.2. Visual interest

The radial plots shown in Figure 10 illustrate the results for mSC, plotted across each of the 18 radial

view directions in 2-hour increments from 8h to 18h on each of the four selected dates. As 8h on

January 13 falls before sunrise and 18h falls beyond sunset, these instances have been excluded for the

visual interest assessment. The results show a clear sensitivity to the architectural composition of this

indoor space, with interest predictions of excitement generally higher towards the East and West

corners, where there is an increased frequency of window openings resulting in direct sunlight

penetration. There is also a visible impact of sky condition, as overcast scenes are generally predicted to be less extreme in excitement and more calming or neutral than the same instance rendered with a clear sky scene.

While it is interesting to see the difference between sky conditions, it is equally informative to see how dynamic sun positions affect predictions of visual interest over time. If we look at the radial plot for February 28 at 8h, we can see that the overcast sky condition remains calming or neutral in all view directions, while the clear sky condition results in an exciting response throughout those view directions oriented North. The radial plot for April 14 at 8h shows a similar trend, with exciting responses higher towards the Northeast, where sun angles have penetrated further in through the windows distributed towards sunrise. An opposite response can be seen on May 30 at 18h, where the most exciting view directions are predicted towards the Southwest, where sunset angles have a greater effect in the field-of-view.
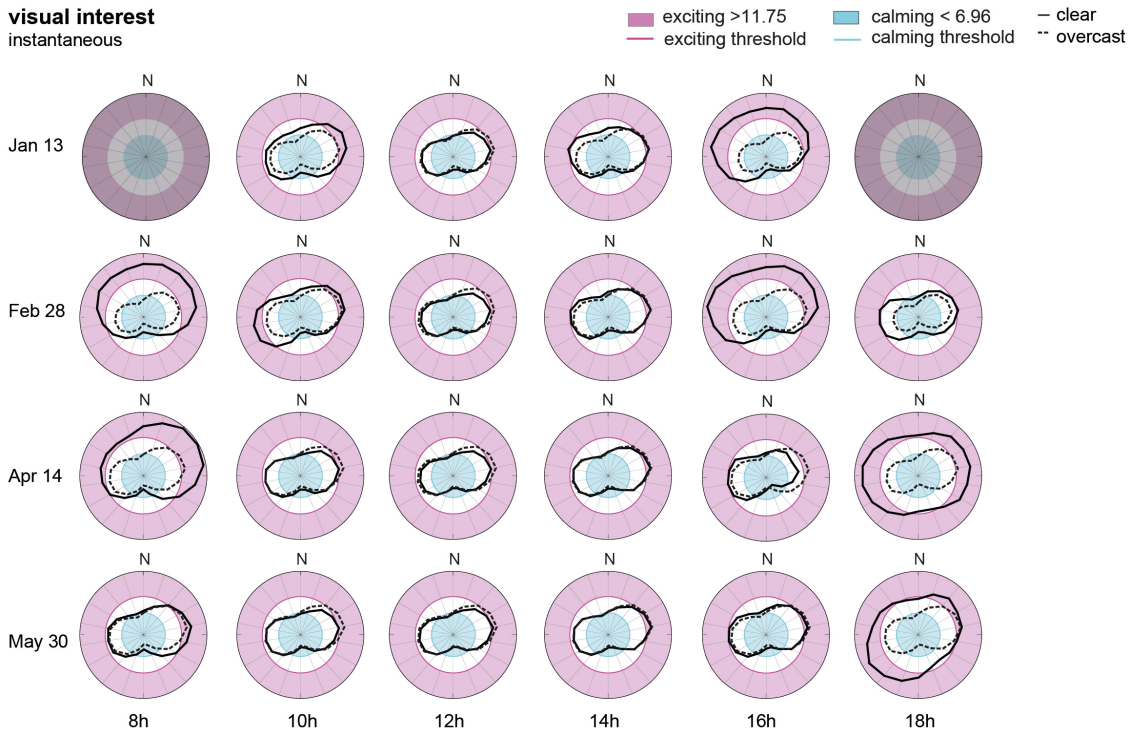

Figure 10 – Radial plots showing the results for visual interest. The mSC shown at every 2h and compared against predictions of exciting and calming thresholds obtained from experimental results. The mSC responds to low sun angles as seen under clear sky conditions for January 13, where the overcast sky remains constant over time.

24

4.3. Gaze responsive zones

The radial plots in Figure 11 illustrate the 'gaze responsive' results. Each plot shows the angular

distribution of the 3D mapping for 'shifted' view directions. The 'shifted' view directions are obtained

by applying the GR_L model on the initial 18 initially given view directions over the 360° of space with

20° intervals to illustrate the gaze responsive outputs. This 3D mapping of the gaze directions on

cylindrical coordinate system are obtained using the inverse tangent transformation of the generated

gaze responsive vectors coordinates. In order to achieve a representative group size of the 18 'shifted'

gaze directions, we grouped the data in 6 bins to determine the dominant 'gaze responsive zones'.

These results are presented for 4 days of the year under overcast and clear sky conditions.

Spatial zones that gaze responds to as a result of avoiding largest contrast variations in the

field of view from one view point in space can be identified over time. An explorative analysis of the

results shows that the spatial composition of the architectural case study has a noticeable influence on

the gaze responsive zone directions, while time of day has a minimal effect. In other words, the higher

contrasts captured by the GR_L model have caused gaze shifts over space, resulting in more frequent

gaze responses whereas contrast variations have changed over time in a constant manner and result in

a lower influence on gaze shifts. To quantify this observation, a two way ANOVA was done on the

frequency of gaze responses. The factors used were spatial configuration (6 bins representing 60° of

angular divisions) and time of the day (6 time points during the day from 8h to 18h with 2 hours

interval) for each sky type (clear and overcast). The 6 spatial bins were chosen to ensure a minimum

of 3 view direction in every bin in case of even angular distribution. The results show that under clear

sky conditions there is a main effect of spatial configuration ($F_{5,120} = 30.36$, p<0.001) while time of

the day has no significant effect on the gaze response frequency ($F_{5,120} = 0.55$, p=0.904). The effect

of spatial configuration under overcast sky conditions is lower than under clear sky conditions

($F_{5,120} = 16.91$, p<0.001), while time of day has a higher effect on gaze variations ($F_{5,120} = 4.87$,

p<0.001). This is mainly caused by lower luminance contrasts variation during wintertime under

overcast sky conditions where gaze responses have been lower. The dominant gaze responsive zone is

mainly directed towards the Northwest and is independent of the time of the day. This result highlights

the importance of architectural design on façade and space layout on our gaze responses. Access to such information in the design phase can assist the designer to reevaluate and rethink the design to adapt best to the architectural program of the space.
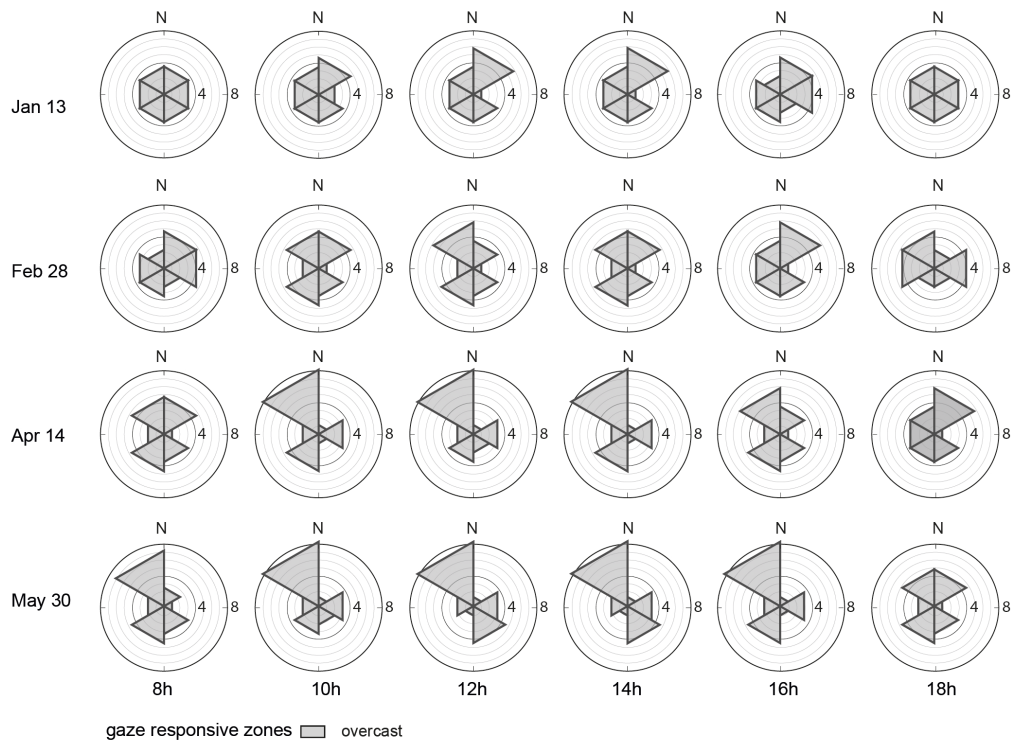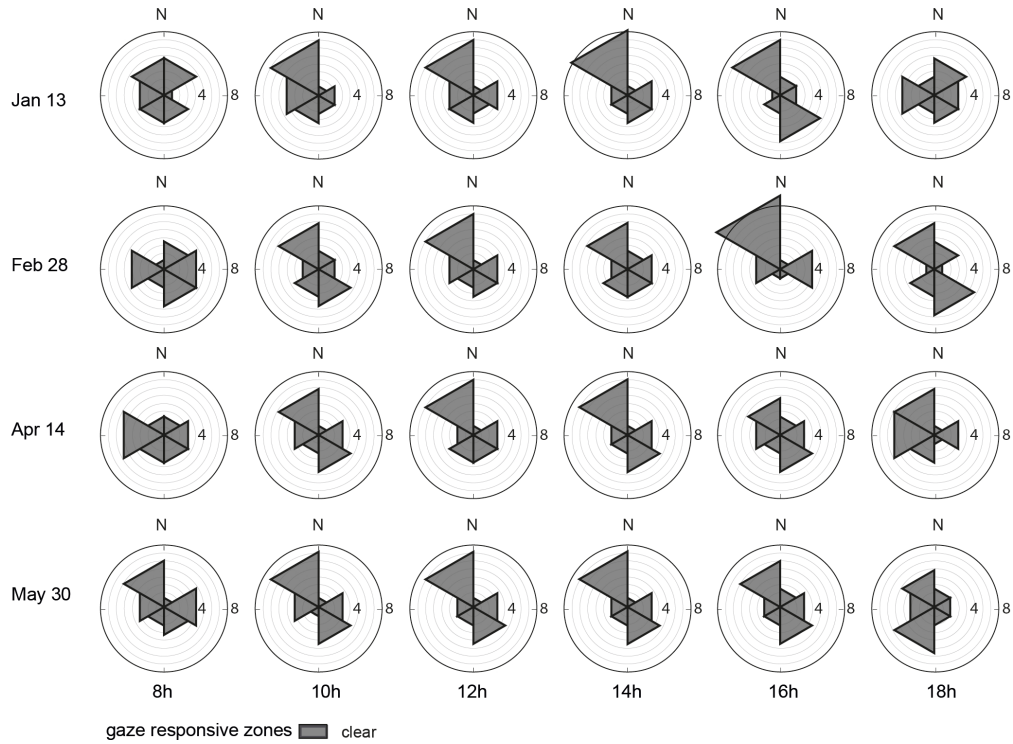
Figure 11 – Frequency of responsive view directions resulting from the light-driven gaze response model under clear and overcast sky conditions.

4.4. Comparative analysis

While future work in this line of research may indeed seek to combine these three novel performance indicators into a composite model for multi-criteria human-centric evaluation, this paper takes a more parallel comparative approach. Through a streamlined workflow and parallel analysis, immersive daylight renderings have been used to assess non-visual health potential, perceptual interest, and gaze behavior across the space of a selected building from the perspective of an occupant. For each view direction under each sky condition and instance of time, we can compare the resulting model predictions and discuss which directions induce visual interest, while avoiding high luminance contrasts, and provide adequate ocular exposure to induce direct non-visual effects.

For each date selected in this analysis, Figure 12(a) shows the cumulative daily response over bi-hourly increments for both clear and overcast sky conditions. While the clear sky predictions are mostly symmetrical, there is variation over the year as a higher cumulative dose is achieved in the summer when illuminance values are high. In contrast, overcast sky predictions vary substantially between months and across view directions (Figure 12(a)). This asymmetry can be attributed to the distribution of windows, which is most concentrated in the East and West directions. Although the recommended threshold of health potential is never fully achieved throughout the day on January 13, it is only partially achieved on February 28 in select view directions (namely towards the east and west).

While non-visual responses are most useful to discuss through their cumulated effect over time (as the nvR_D model is dependent on duration and history of light exposure), perceptual effects are less intuitive when reduced from point-in-time instances to daily averages or a sum. When we observe perceptual dynamics across a series of hourly instants, we can illustrate the impact of variable sun angles on predictions of excitement instantaneously. If, however, we want to draw more general conclusions about the strength and frequency of perceptual responses across the day as a result of architectural composition, a daily sum of mSC under clear and overcast sky conditions can show trends by view direction. For example, Figure 12(b) shows that the difference between clear and overcast skies is more pronounced in the winter months and almost indistinguishable by May 30 as the sun angles ascend, driving less direct sunlight into the side-lit windows. This daily sum also reveals

that East and West view directions predict consistently higher perceptual excitement under all sky conditions, due in large part to the distribution of windows.

Daily analyses for health potential and visual interest find consensus on view direction that appear to induce stronger non-visual and perceptual responses, but like all multi-criteria assessments, the gaze-response model reveals a third and critically important dimension with implications to actual gaze responses as a function of luminance contrast. Higher luminance contrasts levels in the East and West directions are predicted to cause a shift in gaze responses, primarily in the Northwest direction. This composite illustration of data across multiple dimensions of time, sky, and, view direction provides the designer with three important but sometimes conflicting occupant-centric performance outputs which must be considered strategically depending on space function and design intent. The frequency of light-driven gaze responses across the day predicts a dominant gaze responsive zone towards the Northwest (with an opening span of 80°) with 61-83% and 71% gaze encounter under respectively clear and overcast sky conditions. Beside the South orientation for both clear and overcast sky with frequency of 52%, the other orientations show below 45% of gaze encounter (Figure 12(c)).

The most 'stimulating' view directions for health and interest seem to be East and West, but gaze behavior is predicted to shift the dominant view directions towards Northwest. Using this assessment, one could begin to consider which directions and/or façade conditions may be appropriate for task-oriented activities (such as office work), while others could be more appropriate for social activities, where visual comfort may be less desirable than perceptual stimulation.
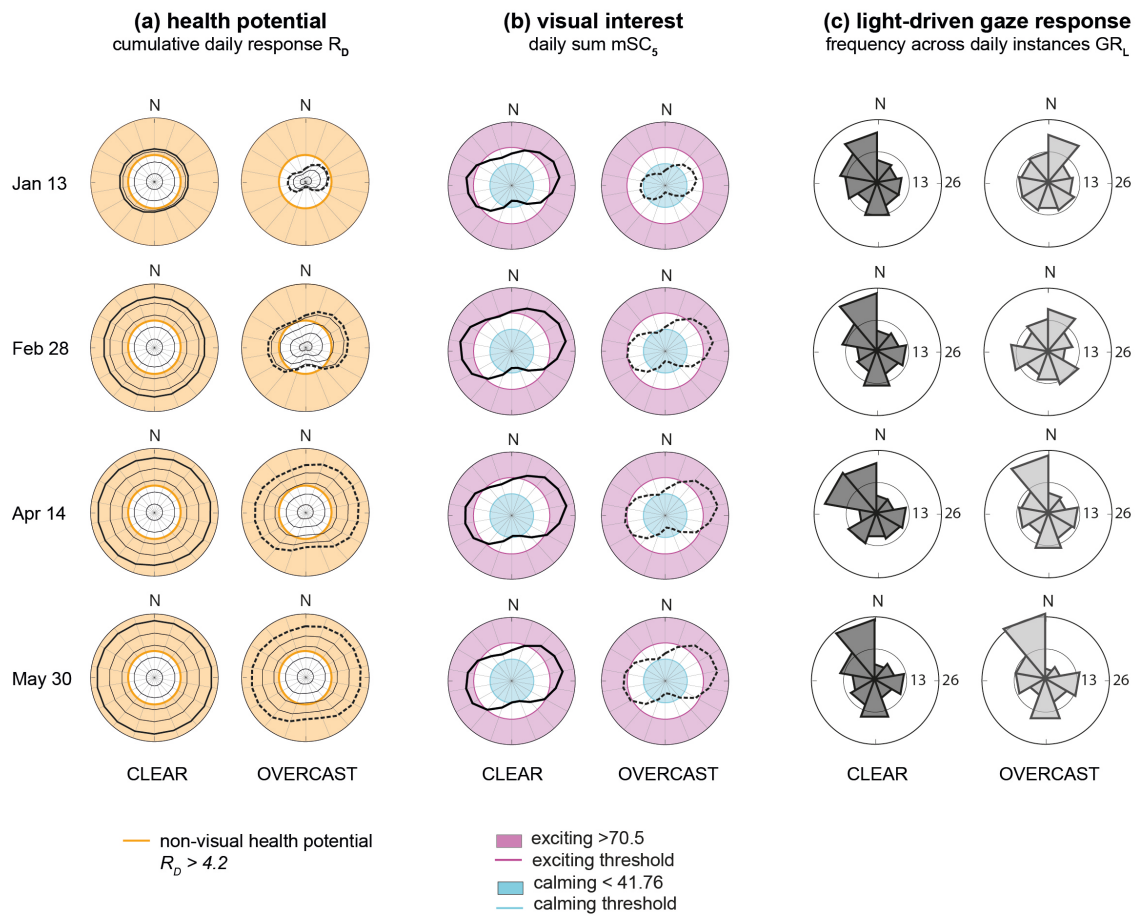
Figure 12 – Comparison of the three novel performance indicators for clear and overcast sky conditions. (a) The accumulation of the relative non-visual response is shown at every 2h increment to illustrate the rate of accumulation towards achieving the health potential of each view direction. (b) The daily sum of modified spatial contrast by view direction. (c) The overall frequency of gaze response grouped into 9 equal bins. The maximum frequency of 26 is obtained for May 30 towards Northwest compared to the 'unresponsive frequency' of 12.

5. Discussion

The focus of this paper was to demonstrate the pertinence and complementarity potential of integrating human visual and non-visual responses regarding daylighting performance into a common workflow to improve our understanding of these responses which happen at the eye-level. While the proposed workflow was applied to a single viewpoint in space, the authors acknowledge that occupant behavior is obviously not restricted to a singular view position and would require a series of inputs to account

for the visual immersion of an occupant in space over time. Based on a generalizable schedule for a single occupant or group of occupants, the future integration of spatial, temporal, and task inputs could be integrated within this workflow and provide a more accurate assessment of behavior and performance impacts at the occupant level.

It is important for the sake of discussion to reiterate that the work presented in this paper is based on parallel and comparative analyses. While we cannot yet assess the possible interactions, if any, between the models introduced in this paper, we can discuss daylight performance with an expanded perspective, accounting for characteristics of health, perception and behavior which have not been previously considered. Due to the parallel nature of the workflow presented here, it may not always be possible to achieve desired goals for all three performance indicators as humans have conflicting needs and wants regarding daylight. Depending on the intentions of the architect and/or lighting designer, a trade-off must then be made to prioritize the user depending on architectural program or specific occupants needs. For example, an office or classroom, where occupants spend long periods of time seated with a static task orientation may prioritize gaze responses due to discomfort avoidance and health potential. On the other hand, a lobby, atrium, or retail shop may choose to prioritize visual interest over health due to relatively short durations of occupancy and no fixed task orientation.

The limitations associated with this approach hold true in most multi-criteria assessments when two or more analysis methods, like those derived for illumination and fixed field-of-view glare predication, are brought together to make generalized assumptions about daylight performance. Applying a parallel and comparative analysis at the occupant level, such as the workflow introduced by this paper, could help designers test different building design options and develop a better understanding of the temporal and spatial impacts of architectural composition on human responses to light.

In order to move beyond a parallel and comparative analysis and into a truly integrated approach, the next step would be to develop a multi-criteria daylighting performance assessment using the three models introduced in Section 2 and applied in Section 4. To achieve this, the specific

limitations of each model must be defined through further development in each research topic, especially as they pertain to validation and application:

- The non-visual direct-response model is currently based on data collected in controlled laboratory settings and has not yet been validated in real-world conditions. The generalizability of results to different populations is likely to present a further limitation as age and gender may affect non-visual responses to light differently.

- Visual interest predictions were developed based on subjective ratings of 2D images. Forthcoming research in this area will explore subjective assessments using immersive 3D renderings as well as various tone-mapping operators to ensure an accurate representation of lighting levels.

- The preliminary gaze response model presented here is based on predictive avoidance behavior. This model in its current state does not include aspects of space such as view outside of the window that could potentially override the effect of lighting distribution in the field-of-view. The low R^2 value also indicates that while observing a strong shift from the glary situations in the study behind, the linear regression approach that has been adopted here is not the best solution to treat the observed behavioral pattern for a predictive model.

Given that these models were developed using different experimental settings, their generalizability to other lighting conditions and/or occupancy situations needs further investigation. As is true with all daylight performance metrics, prediction models are initially extracted from constrained experimental settings and need additional development to ensure their successful transfer to a wider range of light distributions, and temporal dynamics (i.e side lit office to more complex fenestration types).

Future work in this line of research may indeed seek to explore the inter-relations of predicted performance modules and combine these three novel performance indicators into a composite model for multi-criteria human-centric evaluation. A cross comparison of the three performance indicators can already suggest that gaze responsiveness in relation to visual interest can ensure comfortable, yet exciting daylit spaces. Furthermore, the integration of responsive gaze as input for a dynamic time series driven by program use or occupancy scheduling for the prediction of cumulative non-visual response could provide new insights into the analysis and design of architecture. With an increased

understanding of dynamic lighting environments, human behavior, and responses to health and well-being, we can produce better predictions regarding the benefits of daylight and eventually, their integration within the design process.

6. Conclusion

While each architectural case study must be evaluated to address the specific design intent of the architect or lighting designer, daylight performance is too often reduced to a series of simplified metrics without a nuanced understanding of the relationship between complimentary or conflicting performance goals. In this paper, the authors have brought together three daylight performance indicators, including non-visual health potential, visual interest, and gaze behavior, into a common evaluation and visualization framework through which performance can be assessed through novel and dynamic interpretations of daylight. These chosen indicators have been developed in three separate and parallel studies where human physiological responses, subjective responses, and physiological gaze responses were observed in relation to light and contrast variation in the field-of-view received at the eye level. Data pertaining to non-visual physiological responses was obtained from multiple studies conducted in a controlled laboratory; gaze behavior data was collected in a side-lit office environment while perceptual interest ratings were collected from architectural renderings from a range of spaces using an online survey.

Using these models, we assessed the spatial and temporal daylight performance of a selected case study with a human-centric simulation approach. A novel simulation workflow was proposed using an immersive spatial approach to predict ocular light over 18 view directions on a 360° angular span, which allows for a reduced computational time compared to rendering a new image for each view direction. The obtained photometric values from the lighting simulations were then used as input to three models, allowing us to compare the daylighting performance for non-visual, perceptual, and gaze responses. The results were presented using angular plots to represent the data across all view directions and then replicated for different times and days to understand the temporal effect of lighting from a single location in space for two extreme lighting conditions (overcast and clear sky). An explorative analysis of the results shows that lighting distribution has an influence on all three of the

performance indicators, while time of the day has an insignificant effect on gaze responses. The comparative analysis, conducted on an university building by SANAA chosen as the case study, revealed a consensus on East and West view directions that appear to induce stronger non-visual and perceptual responses, while the dominant 'gaze responsive zones' are mainly directed towards the Northwest. Comparing these predicted human responses through a coordinated simulation approach, we can create a more holistic understanding of daylight and its impact on health, perception, and behavioral gaze responses.

Acknowledgements

Funding

References

[1] R. J. Cole, D. F. Kripke, J. Wisbey, W. J. Mason, W. Gruen, P. J. Hauri, and S. Juarez, "Seasonal variation in human illumination exposure at two different latitudes," *J. Biol. Rhythms*, vol. 10, no. 4, pp. 324–334, Dec. 1995.

[2] S. J. Crowley, T. A. Molina, and H. J. Burgess, "A week in the life of full-time office workers: Work day and weekend light exposure in summer and winter," *Applied Ergonomics*, vol. 46, Part A, pp. 193–200, Jan. 2015.

[3] M. Hébert, M. Dumont, and J. Paquet, "Seasonal and diurnal patterns of human illumination under natural conditions," *Chronobiol. Int.*, vol. 15, no. 1, pp. 59–70, Jan. 1998.

[4] T. Roenneberg, K. V. Allebrandt, M. Merrow, and C. Vetter, "Social Jetlag and Obesity," *Current Biology*, vol. 22, no. 10, pp. 939–943, May 2012.

[5] S. Pauley, "Lighting for the human circadian clock: recent research indicates that lighting has become a public health issue," *Medical Hypotheses*, vol. 63, no. 4, pp. 588–596, 2004.

[6] C. Cajochen, "Alerting effects of light," *Sleep Medicine Reviews*, vol. 11, no. 6, pp. 453–464, Dec. 2007.

[7] S. W. Lockley, "Circadian Rhythms: Influence of Light in Humans," in *Encyclopedia of Neuroscience*, L. R. Squire, Ed. Oxford, UK: Academic Press, 2009, pp. 971–988.

[8] J. J. Vos, "Reflections on glare," *Lighting Research and Technology*, vol. 35, no. 2, pp. 163–176, Jun. 2003.

[9] J. Wienold and J. Christoffersen, "Evaluation methods and development of a new glare prediction model for daylight environments with the use of CCD cameras," *Energy and Buildings*, vol. 38, no. 7, pp. 743–757, Jul. 2006.

[10] J. A. Jakubiec and C. F. Reinhart, "The 'adaptive zone' – A concept for assessing discomfort glare throughout daylit spaces," *Lighting Research and Technology*, vol. 44, no. 2, pp. 149–170, Jun. 2012.

[11] M. Sarey Khanie, J. Stoll, W. Einhäuser, J. Wienold, and M. Andersen, "Gaze responsive visual comfort: new findings on gaze behaviour in a daylit office space in relation to glare," in *Proceddings of CIE 2016 "Lighting Quality and Energy Efficiency,"* Melbourne, Australia, 3-5 March, pp. 373–382.

[12] M. Sarey Khanie, J. Stoll, S. Mende, J. Wienold, W. Einhäuser, and M. Andersen, "Investigation of gaze patterns in daylit workplaces: using eye-tracking methods to objectify view direction as a function of lighting conditions," in *Proceedings of CIE Centenary Conference" Towards a New Century of Light,"* 2013, pp. 250–259.

[13] M. Sarey Khanie, J. Stoll, S. Mende, J. Wienold, W. Einhäuser, and M. Andersen, "Uncovering relationships between view direction patterns and glare perception in a daylit workspace," in *LUXEUROPA*, 2013.

[14] L. Itti, C. Koch, and E. Niebur, "A Model of saliency-based visual attention for rapid scene analysis," *IEEE Transactions on pattern Analysis and Machine intelligence*, vol. 20, no. 11, pp. 1254–1259, 1998.

[15] M. L. Amundadottir, "Light-driven model for identifying indicators of non-visual health potential in the built environment," Ecole polytechnique fédérale de Lausanne, Lausanne, Switzerland, 2016.

[16] S. Rockcastle, M. L. Amundadottir, and M. Andersen, "Contrast measures for predicting perceptual effects of daylight in architectural renderings," *Lighting Research and Technology*, published online before print, Apr. 2016.

[17] M. Sarey Khanie, "Human responsive daylighting in offices: a gaze-driven approach for dynamic discomfort glare assessment," Ecole polytechnique fédérale de Lausanne, Lausanne, Switzerland, 2015.

[18] M. A. Steane, *The Architecture of Light: Recent Approaches to Designing with Natural Light*. Routledge, 2011.

[19] J. Pallasmaa, *The Eyes of the Skin: Architecture and the Senses*, 3rd ed. John Wiley & Sons, 2012.

[20] S. Holl, S. Kwinter, and J. Safont-Tria, *Steven Holl: Color, Light, Time*. Ls Müller, 2012.

[21] K. Steemers and M. A. Steane, *Environmental Diversity in Architecture*. London and New York: Routledge, 2012.

[22] J. Phipps-Nelson, J. R. Redman, D.-J. J. Dijk, and S. M. Rajaratnam, "Daytime exposure to bright light, as compared to dim light, decreases sleepiness and improves psychomotor vigilance performance.," *Sleep*, vol. 26, no. 6, pp. 695–700, Sep. 2003.

[23] M. Rüger, M. C. Gordijn, D. G. Beersma, B. de Vries, and S. Daan, "Time-of-day-dependent effects of bright light exposure on human psychophysiology: comparison of daytime and nighttime exposure.," *American journal of physiology. Regulatory, integrative and comparative physiology*, vol. 290, no. 5, pp. R1413–R1420, May 2006.

[24] A. U. Viola, L. M. James, L. J. Schlangen, and D.-J. J. Dijk, "Blue-enriched white light in the workplace improves self-reported alertness, performance and sleep quality.," *Scandinavian journal of work, environment & health*, vol. 34, no. 4, pp. 297–306, Aug. 2008.

[25] G. Vandewalle, S. Gais, M. Schabus, E. Balteau, J. Carrier, A. Darsaud, V. Sterpenich, G. Albouy, D. J. Dijk, and P. Maquet, "Wavelength-dependent modulation of brain responses to a working memory task by daytime light exposure," *Cerebral Cortex*, vol. 17, no. 12, pp. 2788–2795, Dec. 2007.

[26] J. M. Zeitzer, D.-J. Dijk, R. E. Kronauer, E. N. Brown, and C. A. Czeisler, "Sensitivity of the human circadian pacemaker to nocturnal light: melatonin phase resetting and suppression," *The Journal of Physiology*, vol. 526, no. 3, pp. 695–702, Aug. 2000.

[27] C. Cajochen, M. Münch, S. Kobialka, K. Kräuchi, R. Steiner, P. Oelhafen, S. Orgül, and A. Wirz-Justice, "High sensitivity of human melatonin, alertness, thermoregulation, and heart rate to short wavelength light.," *J Clin Endocrinol Metab*, vol. 90, no. 3, pp. 1311–1316, Mar. 2005.

[28] S. L. Chellappa, R. Steiner, P. Blattner, P. Oelhafen, T. Götz, and C. Cajochen, "Non-Visual Effects of Light on Melatonin, Alertness and Cognitive Performance: Can Blue-Enriched Light Keep Us Alert?," *PLoS ONE*, vol. 6, no. 1, p. e16429, Jan. 2011.

[29] S. W. Lockley, E. E. Evans, F. A. Scheer, G. C. Brainard, C. A. Czeisler, and D. Aeschbach, "Short-wavelength sensitivity for the direct effects of light on alertness, vigilance, and the waking electroencephalogram in humans.," *Sleep*, vol. 29, no. 2, pp. 161–168, Feb. 2006.

[30] G. Vandewalle, C. Schmidt, G. Albouy, V. Sterpenich, A. Darsaud, G. Rauchs, P.-Y. Berken, E. Balteau, C. Degueldre, A. Luxen, P. Maquet, and D.-J. Dijk, "Brain Responses to Violet, Blue, and Green Monochromatic Light Exposures in Humans: Prominent Role of Blue Light and the Brainstem," *PLoS ONE*, vol. 2, no. 11, p. e1247, Nov. 2007.

[31] I. Provencio, I. R. Rodriguez, G. Jiang, W. P. Hayes, E. F. Moreira, and M. D. Rollag, "A novel human opsin in the inner retina," *J. Neurosci.*, vol. 20, no. 2, pp. 600–605, Jan. 2000.

[32] M. Hébert, S. K. Martin, C. Lee, and C. I. Eastman, "The effects of prior light history on the suppression of melatonin by light in humans.," *Journal of pineal research*, vol. 33, no. 4, pp. 198–203, Nov. 2002.

[33] S. A. Jasser, J. P. Hanifin, M. D. Rollag, and G. C. Brainard, "Dim Light Adaptation Attenuates Acute Melatonin Suppression in Humans," *Journal of Biological Rhythms*, vol. 21, no. 5, pp. 394–404, Oct. 2006.

[34] A.-M. M. Chang, F. A. Scheer, and C. A. Czeisler, "The human circadian system adapts to prior photic history.," *The Journal of physiology*, vol. 589, no. 5, pp. 1095–1102, Mar. 2011.

[35] K. A. Smith, M. W. Schoen, and C. A. Czeisler, "Adaptation of Human Pineal Melatonin Suppression by Recent Photic History," *Journal of Clinical Endocrinology & Metabolism*, vol. 89, no. 7, pp. 3610–3614, Jul. 2004.

[36] C. Gronfier, K. P. Wright, R. E. Kronauer, M. E. Jewett, and C. A. Czeisler, "Efficacy of a single sequence of intermittent bright light pulses for delaying circadian phase in humans," *American Journal of Physiology - Endocrinology And Metabolism*, vol. 287, no. 1, pp. E174–E181, Jul. 2004.

[37] A.-M. M. Chang, N. Santhi, M. A. St. Hilaire, C. Gronfier, D. S. Bradstreet, J. F. Duffy, S. W. Lockley, R. E. Kronauer, and C. A. Czeisler, "Human responses to bright light of different durations.," *The Journal of physiology*, vol. 590, no. 13, pp. 3103–3112, Jul. 2012.

[38] J. J. Gooley, S. M. W. Rajaratnam, G. C. Brainard, R. E. Kronauer, C. A. Czeisler, and S. W. Lockley, "Spectral responses of the human circadian system depend on the irradiance and duration of exposure to light," *Sci Transl Med*, vol. 2, no. 31, p. 31ra33, May 2010.

[39] M. L. Amundadottir, L. Lockley Steven, and M. Andersen, "Unified framework to evaluate non-visual spectral effectiveness of light for human health," *Lighting Res. Technol.*, published online before print, Jun. 2016.

[40] M. L. Amundadottir, M. A. St. Hilaire, S. W. Lockley, and M. Andersen, "Modeling non-visual responses to light: unifying spectral sensitivity and temporal characteristics in a single model structure," in *CIE Centenary Conference "Towards a New Century of Light,"* Paris, France, 2013, vol. CIE x038:2013, pp. 101–110.

[41] D. W. Rimmer, D. B. Boivin, T. L. Shanahan, R. E. Kronauer, J. F. Duffy, and C. A. Czeisler, "Dynamic resetting of the human circadian pacemaker by intermittent bright light.," *American journal of physiology. Regulatory, integrative and comparative physiology*, vol. 279, no. 5, Nov. 2000.

[42] K. Parpairi, N. V. Baker, K. A. Steemers, and R. Compagnon, "The Luminance Differences index: a new indicator of user preferences in daylit spaces," *Lighting Research and Technology*, vol. 34, no. 1, pp. 53–66, Mar. 2002.

[43] K. V. D. Wymelenberg, M. Inanici, and P. Johnson, "The Effect of Luminance Distribution Patterns on Occupant Preference in a Daylit Office Environment," *LEUKOS*, vol. 7, no. 2, pp. 103–122, Sep. 2013.

[44] C. Demers, "Assessing light in architecture: a numerical procedure for a qualitative and quantitative analysis," in *Proceedings of the Italian Lighting Association (AIDI)*, 2006.

[45] G. R. Newsham, C. Richardson, C. Blanchet, and J. A. Veitch, "Lighting quality research using rendered images of offices," *Lighting Research and Technology*, vol. 37, no. 2, pp. 93–112, Jun. 2005.

[46] S. Rockcastle and M. Andersen, "Measuring the dynamics of contrast & daylight variability in architecture: A proof-of-concept methodology," *Building and Environment*, vol. 81, pp. 320–333, Nov. 2014.

[47] A. Rizzi, T. Algeri, G. Medeghini, and D. Marini, "A proposal for contrast measure in digital images," in *Conference on Colour in Graphics, Imaging, and Vision*, 2004, pp. 187–192.

[48] R. Hopkinson, "The multiple criterion technique of subjective appraisal," *Quarterly Journal of Experimental Psychology*, vol. 2, no. 3, pp. 124–131, 1950.

[49] S. Kokoschka and P. Haubner, "Luminance ratios at visual display workstations and visual performance," *Lighting research and Technology*, vol. 17, no. 3, pp. 138–144, 1985.

[50] S. Guth, "Light and comfort.," *Industrial medicine & surgery*, vol. 27, no. 11, pp. 570–574, 1958.

[51] W. Kim and Y. Koga, "Effect of local background luminance on discomfort glare," *Building and Environment*, vol. 39, no. 12, pp. 1435–1442, 2004.

[52] C. CIBSE, "Code for interior lighting," *London: The Chartered Institution of Building Services Engineers*, 1994.

[53] Y. Lin, S. Fotios, M. Wei, Y. Liu, W. Guo, and Y. Sun, "Eye movement and pupil size constriction under discomfort glare," *Investigative ophthalmology & visual science*, vol. 56, no. 3, pp. 1649–1656, 2015.

[54] J. A. Yamin Garretón, R. G. Rodriguez, A. Ruiz, and A. E. Pattini, "Degree of eye opening: A new discomfort glare indicator," *Building and Environment*, vol. 88, pp. 142–150, Jun. 2015.

[55] A. Nuthmann and W. Einhäuser, "A new approach to modeling the influene of image features on fixation selection in scenes.," *The New York Academy of Scientists*, In press.

[56] P. M. Sury, S. Hubalek, and C. Schierz, *A first step on eye movements in office settings: Eine explorative Studie zu Augenbewegungen im Büroalltag*, vol. 51. GRIN Verlag, 2010.

[57] B. T. Vincent, R. Baddeley, A. Correani, T. Troscianko, and U. Leonards, "Do we look at lights? Using mixture modelling to distinguish between low-and high-level factors in natural image viewing," *Visual Cognition*, vol. 17, no. 6–7, pp. 856–879, 2009.

[58] S. Hubalek and C. Schierz, "LichtBlick–photometrical situation and eye movements at VDU work places," in *CIE Symposium*, 2004, vol. 4, pp. 322–324.

[59] M. Sarey Khanie, J. Stoll, W. Einhäuser, J. Wienold, and M. Andersen, "Gaze and discomfort glare, Part 1: Development of a gaze-driven photometry," *Lighting Research and Technology*, published online before print, Jun. 2016.

[60] J. Schanda, T. Bristow, Carter, E. Chain, M. K. Gunde, R. Hirschler, B. Jordan, C. Kim, E. Pierson, M. R. Pointer, K. Richter, G. Roesler, T. Tarczali, J. van Kemenade, and J. Zwinkels, "CIE 184:2009 Indoor daylight illuminants," CIE, 2009.

[61] J. Wienold and J. Christoffersen, "Evaluation methods and development of a new glare prediction model for daylight environments with the use of CCD cameras," *Energy and Buildings*, vol. 38, no. 7, pp. 743–757, Jul. 2006.

[62] M. Sarey Khanie, J. Wienold, and M. Andersen, "A sensitivity analysis on glare detection parameters," presented at the BS 2015: 14th International Conference of the International Building Performance Simulation Association, 2015.

[63] C. Cajochen, J. M. Zeitzer, C. A. Czeisler, and D.-J. Dijk, "Dose-response relationship for light intensity and ocular and electroencephalographic correlates of human alertness," *Behavioural Brain Research*, vol. 115, no. 1, pp. 75–83, Oct. 2000.

1. Appendix: supplementary equations

In the following, the mathematical equations of the three models are described.

1.1. Non-visual direct-response (nvR$_D$) model

The non-visual direct-response (nvR$_D$) model is described as follows. The light stimulus $I(t)$, is passed through a linear filter L$_1$, which is associated with the temporal integration of the retina, to determine the output $u(t)$

$$u(t) = \frac{1}{d_1}\sum_{t-d_1}^{t} I(t), \tag{3}$$

where $d_1 = 0.3$ h is the length of filter L$_1$. The time step size Δt is set to a fixed value or equal to 0.1 h. Then $u(t)$ is transformed by a nonlinear function $N(u)$, describing the intensity-response relationship to the light stimulus, to determine the output $v(t)$

$$v(t) = N(u(t)). \tag{4}$$

It is known that the non-visual system exhibits a nonlinear mechanism that controls the responsiveness as a function of light intensity [26], [63]. The relative intensity-response curve (IRC) is described in the nvR$_D$ model by a nonlinear term and adaptive half-maximum function to account for dynamic regulation of non-visual responses

$$N(u(t)) = \left(1 + \left(\frac{\sigma(t)}{u(t)}\right)^n\right)^{-1}, \tag{5}$$

where $n = 3.55$ is the slope and $\sigma(t)$ is the half-maximum function that adapts to contrast in prior light history. A feed-forward mechanism shifts the half-maximum constant for $u_H \geq 0$

$$\sigma(t) = \sigma_0/2, \qquad\qquad \forall u_H(t) < 0, \tag{6}$$

$$\sigma(t) = \sigma_0 \times 2^{u_H(t)-1}, \qquad\qquad \forall u_H(t) \geq 0, \tag{7}$$

where $\sigma_0 = 0.26$ W/m^2 effective and is equivalent to 106 lx for melatonin suppression response [26]. The adaptation to contrast in prior history of light is calculated using a simple moving average

$$u_H(t) = \frac{1}{d_H}\sum_{i=0}^{d_H/\Delta t} \log_{10}(u(t) \times K_m A_v/K_e)\Delta t, \tag{8}$$

where $d_H = 1.7$ h is the width of filter L$_H$. The constant $K_m A_v/K_e = 260.7$ accounts for order of magnitude difference between the conversion from photometric to radiometric quantities.

The signal $v(t)$ is finally passed through a second filter L_2, which reflects the adaptation of the non-visual system to continuous light exposure, to determine the final output $r_D(t)$

$$r_D(t) = \alpha \times v(t-1) + (1-\alpha) \times r_D(t-1), \tag{9}$$

where $\alpha = 2/(d_2 + 1)$ and $d_2 = 2.3$ h represents the length of filter L_2.

1.2. Modified spatial contrast (mSC)

The modified spatial contrast (mSC) in the level N is defined as

$$mSC_N = \frac{1}{WH} \sum_{i=1}^{W_N} \sum_{j=1}^{H_N} c_{i,j}, \tag{10}$$

where $W_N = W_{N-1}/2$ and $H_N = H_{N-1}/2$ are the width and height of the image at level N halved in each subsequent level and $c_{i,j}$ is the contrast of each pixel, calculated as

$$c_{i,j} = \sum_{k \in K_8} \alpha |p_{i,j} - p_k|, \tag{11}$$

where pixels p_k are the 8 neighbouring pixels of $p_{i,j}$ and the weight α applied to each of the 8 surrounding pixels k is

$$\alpha = \frac{1}{4 + 2\sqrt{2}} \begin{bmatrix} \frac{\sqrt{2}}{2} & 1 & \frac{\sqrt{2}}{2} \\ 1 & & 1 \\ \frac{\sqrt{2}}{2} & 1 & \frac{\sqrt{2}}{2} \end{bmatrix}. \tag{12}$$

This weight was taken from the original definition of RAMMG, a multi-level contrast algorithm proposed by [47].

1.3. Gaze response light-driven (GR_L) model

The preliminary light-driven gaze (GR_L) model is described with the equation

$$\Delta\theta_{RG} = \beta_1 + \beta_2 \frac{GI}{L_m \times \Delta\theta_{FG}}, \tag{13}$$

where $\beta_1 = 1.92$ represents the intercept to the y-axis and $\beta_2 = 0.56$ represents the slope. A linear regression was applied to fit these constants to data obtained from the experimental study [12], [13] that includes an analysis of gaze-tracking data and image processing of light information. The goodness-of-fit for the linear model was $R^2 = 0.10$ and the residuals where normally distributed. Despite a low R^2 value, the model is statistically significant with a p-value of 4.45e-05.

The glare impact is calculated as

$$GI = \sum_{i=1}^{n} \frac{L_{s,i} \cdot \omega_{s,i}}{P_i},$$

(14)

where $L_{s,i}$ represents the luminance, $\omega_{s,i}$ represents the solid angle, and P_i represents the position for all glare sources $i = 1, \dots, n$.

The adaptation level is introduced as

$$L_m = \frac{1}{2\pi} \sum_{i=1}^{n} L_{s,i} \cdot \omega_{s,i},$$

(15)

by the average luminance L_m of all pixels in the field-of-view rendered in a wide angle fisheye HDR image.

The distance to glare source $\Delta\theta_{FG}$ is the angular distance between the $\overrightarrow{v_F}$, which is the gaze vector from the camera point-of-view (fixed), and the $\vec{g}$, which is the glare vector from the camera point-of-view vp. It is defined by the dot product

$$\Delta\theta_{FG} = \cos^{-1}[(\vec{g} \cdot \overrightarrow{v_F})/(\|\vec{g}\|\|\overrightarrow{v_F}\|)].$$

(16)

The rotation matrix compromises of a matrix of angular rotations γ, β, and α around the three axes from a defined gaze point vp. It is defined as

$$R_x = \begin{pmatrix} 1 & 0 & 0 \\ 0 & \cos\gamma & -\sin\gamma \\ 0 & \sin\gamma & \cos\gamma \end{pmatrix},$$

(17)

$$R_y = \mathbb{1},$$

(18)

$$R_z = \begin{pmatrix} \cos\alpha & -\sin\alpha & 0 \\ \sin\alpha & \cos\alpha & 0 \\ 0 & 0 & 1 \end{pmatrix},$$

(19)

where γ is a counter-clockwise rotation about the x-axis and α is counter-clockwise rotation about the z-axis. The rotation about y-axis represents a head tilt. The assumption here is that there is no head tilt around the y-axis. These rotations are considered in the processing phase of the gaze data behind the model development. Finally, the coordinate system is defined in a way that y-axis is straight from the gaze point; the positive x-axis is points to the right. Each gaze direction was rotated about the respective relevant axes where the origin is the initial gaze position. The rotation matrix is applied to the initial gaze vectors in order to obtain the responsive gaze.